Article

Decreased cloud cover partially offsets the cooling effects of surface albedo change due to deforestation

Hao Luo ®[1,2] ✉, Johannes Quaas ®[2,3] & Yong Han ®[1,4] ✉

Biophysical processes of forests affect climate through the regulation of surface water and heat fluxes, which leads to further effects through the adjustment of clouds and water cycles. These indirect biophysical effects of forests on clouds and their radiative forcing are poorly understood but highly relevant in the context of large-scale deforestation or afforestation, respectively. Here, we provide evidence for local decreases in global low-level clouds and tropical high-level clouds from deforestation through both idealized deforestation simulations with climate models and from observations-driven reanalysis using space-for-time substitution. The decreased cloud cover can be explained by alterations in surface turbulent heat flux, which diminishes uplift and moisture to varying extents. Deforestation-induced reduction in cloud cover warms the climate, partially counteracting the cooling effects of increased surface albedo. The findings from idealized deforestation experiments and space-for-time substitution exhibit disparities, with global average offsets of, respectively, approximately 44% and 26%, suggesting the necessity for further constraints.

Forests have the capacity to buffer global warming by storing large amounts of carbon from the atmosphere via photosynthesis[1–3]. Alongside the biochemical effects, forests can influence the local and regional climate through biophysical processes, including alterations in land surface water and energy balance[4–7]. On the local scale, the higher albedo and lower evapotranspiration (ET) following deforestation cause either surface cooling or warming, depending on which process holds dominance[8–10]. These cooling or warming impacts have the potential to offset or intensify, respectively, the warming effects connected to the released carbon caused by deforestation[11–16]. Extensive studies on the direct biophysical effects of deforestation on surface temperature have unveiled a latitudinal shift from tropical warming to boreal cooling[8,9,17–19]. Nevertheless, globally, alterations in surface albedo are more prevalent in the direct biophysical temperature response than ET because of its wider-scale impact[17]. This suggests

that the global warming attributed to the biochemical effects of deforestation could potentially be mitigated by the cooling effects resulting from increased surface albedo and consequently altered radiative balance[12,14,16]. Yet, the impact of forest indirect biophysical processes on clouds and their associated radiative balance has not been well addressed, and the assessment of how changes in cloud radiative effects interact with the surface albedo effects remains unquantified. Understanding the response of clouds and their radiative effects to deforestation, however, is crucial due to the overwhelming effect clouds play on the Earth's energy budget. It stands as a major challenge in evaluating land-use-change-driven climate change[20–24].

Observational studies allow for the conclusion that deforestation may predominantly reduce global cloud cover[22,23,25], but with contrasting impacts across various regions[21]. These studies mostly

[1]Advanced Science & Technology of Space and Atmospheric Physics Group (ASAG), School of Atmospheric Sciences, Sun Yat-sen University, 519082 Zhuhai, China. [2]Leipzig Institute for Meteorology, Leipzig University, 04103 Leipzig, Germany. [3]German Centre for Integrative Biodiversity Research (iDiv) Halle-Jena-Leipzig, 04103 Leipzig, Germany. [4]Key Laboratory of Tropical Atmosphere-Ocean System (Sun Yat-sen University), Ministry of Education, 519082 Zhuhai, China. ✉e-mail: hao.luo@uni-leipzig.de; hany66@mail.sysu.edu.cn

1

compare clouds above forests and open land in adjacent geographical units (i.e., space-for-time substitution) and find larger cloudiness over forests. This commonly adopted method assumes that forests and neighboring land units share the same climate background, thereby deducing local effects through distinctions in land surface conditions. Apart from observations-based studies, general circulation models (GCMs) have been widely employed to quantify the impacts of deforestation[26–28]. GCMs show a global average enhancement in cloud cover with deforestation[29]. Unlike the observational studies that concentrate solely on local effects, GCMs probably possess the ability to encompass both local and non-local effects of deforestation. Hence, separating local and non-local effects could facilitate comparisons between these two distinct methods and enhance comprehension of the biophysical mechanisms of deforestation on clouds[24].

Given the essential roles of cloud vertical structures in influencing radiative processes[30,31], a sole concentration on overall cloud cover may be insufficient for a comprehensive analysis of the changes in cloud radiative effects from deforestation. Typically, low, highly reflective clouds have a cooling effect as they reflect solar radiation. In contrast, high, semi-transparent clouds contribute to warming by allowing shortwave radiation to pass through while impeding long-wave radiation[32,33]. The alterations in cloud vertical profiles following deforestation have not received adequate attention, and addressing this gap is essential for gaining a deeper understanding of the consequent changes in cloud radiative effects.

In this study, we approach the evaluations of cloud profiles and associated radiative response to deforestation from two distinct viewpoints: the space-for-time substitution method from observations-driven reanalysis and the idealized deforestation experiments available from GCM simulations. Given that the outcomes from GCMs contain both local and non-local signals, we then isolate the local signals using a chessboard-like method[24,34], enabling a comparative analysis between the two distinct ways. Using both methods, this work consistently indicates a global reduction in low-level clouds and a decline in high-level clouds over tropical regions in response to deforestation. In addition, we explore the potential physical mechanisms through which deforestation induces alterations in cloud profiles, suggesting that changes in turbulent heat flux could be a crucial factor. Finally, we quantify the impact of deforestation on cloud radiative forcing within the Earth-atmosphere system, with findings indicating that the warming effects of clouds, to a substantial extent, counterbalance the cooling effects of surface albedo at a global scale.

Results
Cloud profile changes
Two distinct approaches (see Methods) are employed in this study to assess the potential impact of deforestation on cloud fraction profiles. The first method draws upon five available GCMs (Table S1) participating in the Coupled Model Intercomparison Project Phase 6 (CMIP6)[35]. It entails analyzing the idealized global deforestation simulations (deforest-glob) conducted in the Land Use Model Intercomparison Project (LUMIP)[36], and comparing them against the pre-industrial control simulations (piControl). The second method uses the space-for-time substitution to contrast the multi-year average cloud fraction profiles between the neighboring unaltered forested and unaltered open land grids. In this approach, the potential effects of deforestation on cloud profiles are measured by land cover data from the Moderate Resolution Imaging Spectroradiometer (MODIS) and cloud profiles from the European Centre for Medium-Range Weather Forecasts (ECMWF) fifth reanalysis (ERA5). It should be noted that MODIS only provides data for specific times within the diurnal cycle (morning and noon), which may introduce a low bias on the estimate of forest-cloud impacts in the data[23], compared to the model analysis. One significant drawback of the cloud profile data from active satellites is that they have relatively small footprints and sample sizes. As a

result, data from numerous satellite passes must be averaged or combined to create a product with sufficient coverage. Given the finer spatial resolution of ERA5 cloud profiles, and their much larger coverage, in comparison to the available gridded data derived from active satellite observations, along with the strong correlation exhibited between ERA5 and the observations (Supplementary Fig. 1), we employ long-term ERA5 data instead. The moderate correlations between ERA5 and satellite-retrieved cloud profiles in the boundary layer are caused by two aspects: one is the data quality of ERA5 itself, and another is the limitation of active satellite sensors on the detection of low-level clouds, especially under conditions of thick upper clouds or strong surface returns[37–40]. However, the integration of denser and higher-quality observations over land enhances the accuracy of ERA5 boundary layer cloud data compared to over oceans (Supplementary Fig. 1), thereby better suiting this land-focused study. As GCMs contain both local and no-local effects, we extract the local effects from the total signals (see Methods). Isolating local effects can aid in understanding the biophysical mechanisms of deforestation on clouds. Despite the differing principles behind the two methods, it is noted that the space-for-time substitution also solely considers local effects, allowing for a comparison between these two approaches.

While ref. 28 outlined diverse spatial patterns in how cloud cover responds to deforestation across GCMs in LUMIP, once the local effects are isolated, they reveal consistent spatial patterns (Fig. 1a). This implies that the inconsistencies across models documented by ref. 28 primarily arise from discrepancies in non-local effects. For a quantitative comparison between the GCMs and ERA5, we quantify the sensitivity of the cloud fraction profile to deforestation by calculating the changes in cloud fraction per deforestation fraction. Even with distinct principles, both methods show consistency in this specific change across the spatial distribution regarding cloud vertical profile responses to deforestation (Fig. 1). Globally, cloud cover below 700 hPa decreases in response to deforestation, showing consistency with satellite observations[21–23]. The decrease in tropical cloud cover is restricted to relatively low altitudes according to the ERA5 space-for-time substitution method. The response to deforestation is most pronounced in low-level clouds, with additional reductions found for tropical high-level clouds (higher than 500 hPa). Low-level clouds, which are closely coupled with land surface, form and evolve in response to surface heating, moisture fluxes, and other boundary layer processes[41–43]. Therefore, on a global scale, the impacts of deforestation are expected to be more noticeable on low-level clouds than on high-level clouds. While deep-convection clouds are generally not well-coupled with the surface, surface conditions can influence their initiation[44,45]. Therefore, deforestation is not limited to affecting shallow clouds that are fully coupled to the surface but can also impact deep convective clouds to a certain extent. As a result, the height of deep convective cloud tops can roughly indicate the maximum altitude at which deforestation affects clouds. Since the cloud top height of deep convective clouds varies across regions, with those in tropical regions reaching higher altitudes than those in boreal zones (Supplementary Fig. 2), deforestation is more likely to affect high-level clouds in the tropics.

Discussion of physical mechanisms of forest-cloud impacts
Various biophysical processes are engaged in the interactions between forests and clouds, yet identifying the factors that dictate where cloud enhancement or reduction occurs across global deforested areas has remained unclear[21,22,29]. In terms of the thermodynamics and moisture factors involved in cloud formation, cloud cover in certain areas might be restricted by the heating needed for uplift[46,47]. In others, it might be restricted by the availability of moisture[48]. In the following, we explore these two fundamental factors.

In comparison to forests, open land typically exhibits higher surface albedo (Supplementary Fig. 3) and lower ET (Supplementary
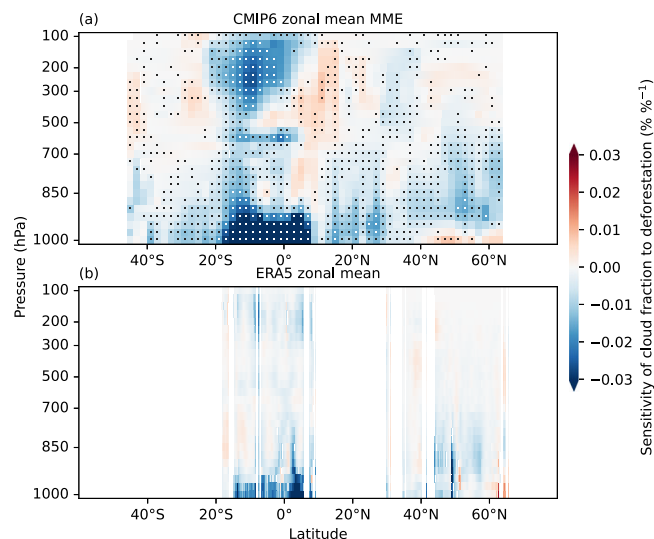
Fig. 1 | Local sensitivity of cloud fraction profile to deforestation. a Zonal mean of the cloud fraction profile difference between the deforest-glob and piControl simulations (deforest-glob minus piControl) per deforestation fraction. The data were the ensemble mean of the local effect extracted from CMIP6 model simulations (see Methods). The stippling represents four or more of the five models showing the same sign. **b** Zonal mean ERA5 cloud fraction profile variations per deforestation fraction using the space-for-time substitution (open land minus forest; see Methods). Only latitudes possessing more than ten available samples are considered to ensure representativeness.

Fig. 4). Increased surface albedo from deforestation causes cooling by reflecting more shortwave radiation. This cooling effect is counterbalanced by lower ET[8]. Both the cooling caused by the surface albedo difference and the warming due to ET difference vary across latitudes, indicating that the magnitude and even the sign of local surface air temperature (SAT) changes resulting from alterations in forests differ across climate regions. When examining SAT changes in deforested areas, shifting from forests to open land induces surface warming in tropical regions (Supplementary Fig. 5). This is primarily due to the prevailing impact of ET on the temperature signal, although alterations in surface albedo partially counteract this surface warming. In contrast, the overall biophysical effect of deforestation leads to surface cooling in the boreal zone from GCMs (Supplementary Fig. 5), which agrees with previous studies from both observations[8,49] and simulations[24,50]. Notably, the impact of surface albedo becomes more pronounced as latitude increases, while the influence of ET tends to diminish with higher latitudes. Hence, in boreal regions, increased surface albedo emerges as the predominant factor of surface cooling. However, surface cooling is not as evident from the space-for-time substitution approach, since SAT is nonlinearly influenced by both radiative and non-radiative processes. Previous observation-based studies also suggest small changes in SAT due to deforestation in boreal regions[51,52].

Moreover, the reduction in incoming solar radiation and the drop in SAT caused by the higher surface albedo results in a substantial decrease in sensible heat flux (SH) within the boreal zone; however, in the tropics, the decline in the surface turbulent heat flux primarily stems from the reduction in latent heat flux (LH) due to the dominant role of ET (Fig. 2). Deforestation increases near-surface wind speed due to a decrease in surface roughness (Supplementary Fig. 6), enhancing the heat and water vapor exchange rate between the surface and the air, thereby increasing turbulent fluxes. Apart from being influenced by the near-surface wind speed, SH and LH, respectively, however, are also related to the temperature and humidity gradients between the surface and the air. The fluxes are proportional to the product of the wind speed and the gradient[53,54]. We find that the decreased
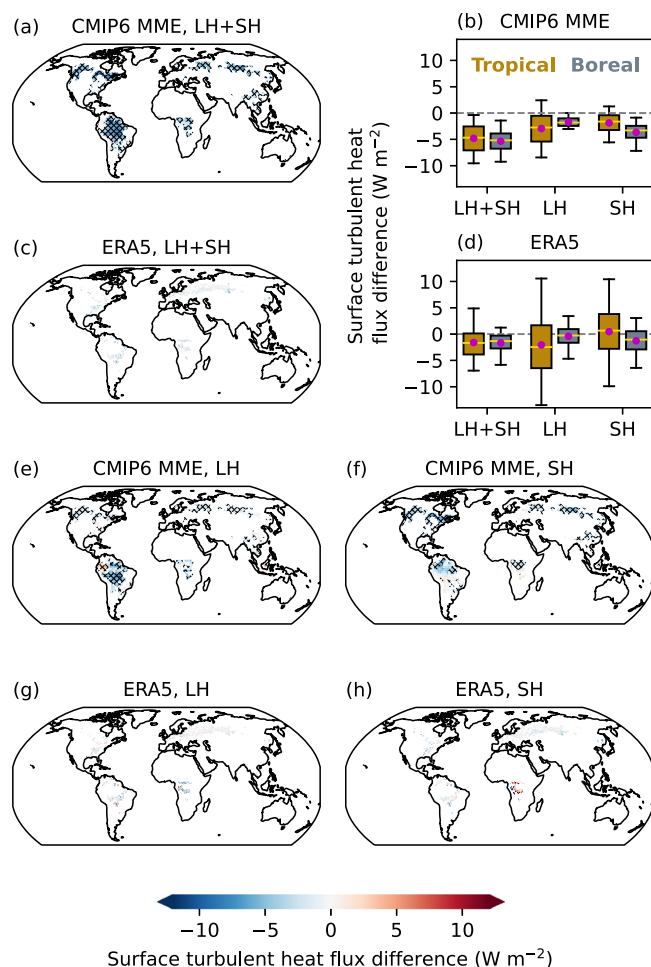
Fig. 2 | Changes in surface turbulent heat fluxes due to deforestation. a Global pattern of the surface turbulent heat flux (latent heat (LH) + sensible heat (SH)) difference between the deforest-glob and piControl simulations (deforest-glob minus piControl). Diagonal hashing indicates four or more of the five models showing the same sign of change. **b** Box plots of the CMIP6 surface turbulent heat flux (LH + SH, LH and SH) differences between the deforest-glob and piControl simulations over both tropical and boreal areas. **c** ERA5 surface turbulent heat flux (LH + SH) variations due to deforestation using the space-for-time substitution (see Methods). **d** Box plots of the ERA5 surface turbulent heat flux (LH + SH, LH and SH) variations due to deforestation. The data in (**a, b**) is the ensemble mean of the local effect extracted from CMIP6 model simulations (see Methods). Boxes in (**b, d**) show the 25th to 75th percentiles of the data, whiskers display the 5th to 95th percentiles, horizontal yellow lines in the boxes represent the median values, and red dots are the mean values. (**e, f**) Same as (**a**) but for LH and SH, respectively. (**g, h**) Same as (**c**) but for LH and SH, respectively.

temperature gradient between the surface and the air in the boreal zones resulting from deforestation outweighs the role of near-surface wind speed (Supplementary Fig. 7), leading to a reduction in SH. Since there is no proxy for the humidity gradient between the surface and the air, we infer changes in humidity gradient from changes in ET. An increase in wind speed is accompanied by a decrease in ET (Supplementary Fig. 4), suggesting that the decreased humidity gradient between the surface and the air caused by deforestation primarily drives the reduction in LH. Thus, when combining the alterations in LH and SH, the decrease in surface turbulent heat flux depicted in Fig. 2 is evident globally. In conclusion, the response of cloud cover to the reduction in turbulent heat flux is illustrated through the decrease in water vapor supply due to decreased LH in the tropics and the weakening in the uplifting process caused by decreased SH in the boreal regions.
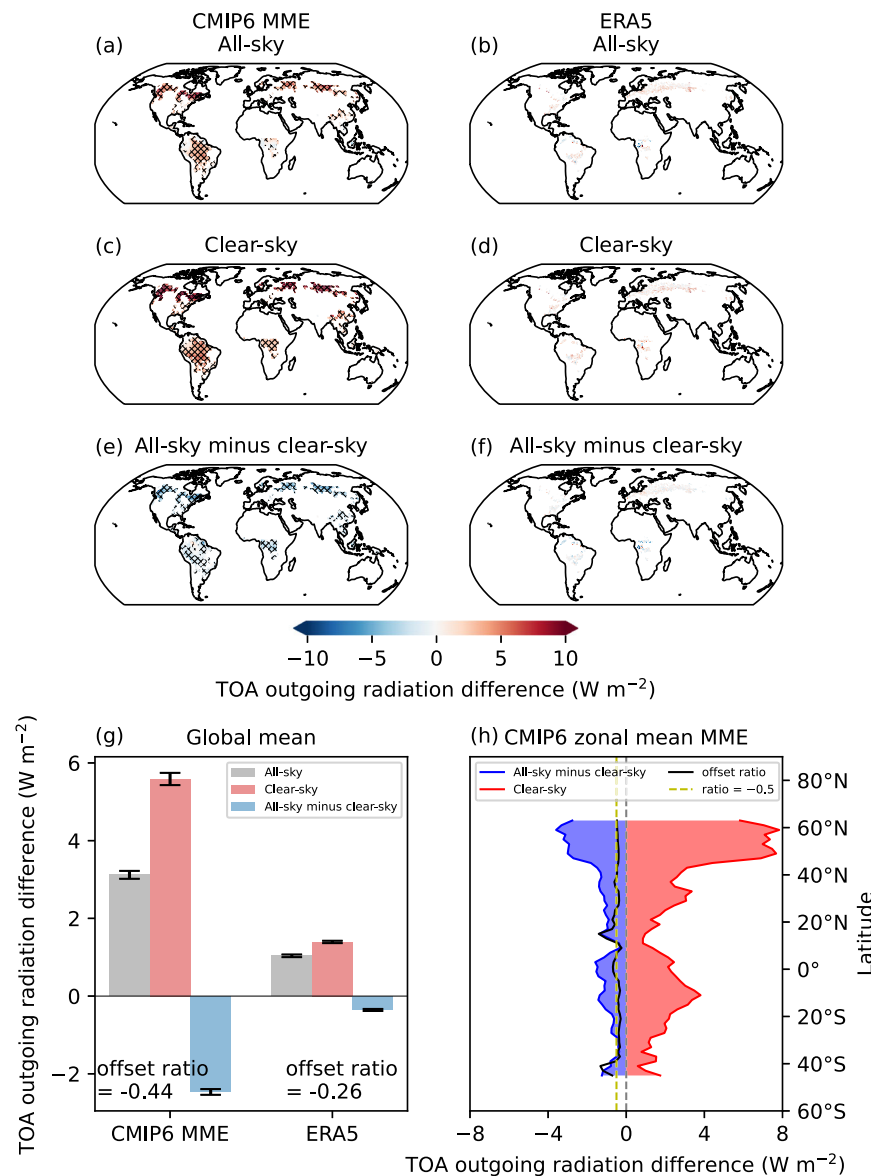
Fig. 3 | Changes in outgoing radiation at the top of atmosphere (TOA) due to deforestation. a, **c**, **e** Global pattern of the TOA outgoing radiation (shortwave + longwave) difference between the deforest-glob and piControl simulations (deforest-glob minus piControl), respectively, under all-sky, clear-sky, and all-sky minus clear-sky circumstances. Diagonal hashing indicates four or more of the five models showing the same sign of change. **b**, **d**, **f** ERA5 TOA outgoing radiation (shortwave + longwave) variations due to deforestation using the space-for-time substitution (see Methods). Global mean values and standard errors for (**a**–**f**) are shown in (**g**). The offset ratio is the proportion of all-sky minus clear-sky to the all-sky value. **h** CMIP6 zonal mean of the TOA outgoing radiation (shortwave + longwave) difference between the deforest-glob and piControl simulations under both clear-sky and all-sky minus clear-sky circumstances. The black line indicates the zonal mean offset ratio and the dashed yellow line is the ratio equal to −0.5. The CMIP6 data were the ensemble mean of the local effect extracted from multi-model simulations (see Methods).

The local effects derived from ERA5 contain both the mean-state difference and the secondary mesoscale circulation (See Methods). While the mean-state difference mechanism has been discussed above, the secondary circulation processes can enhance or inhibit the cloud responses to deforestation[21,23,55]. This secondary circulation-induced cloud change is mainly driven by SH[21], indicating that cloud enhancement occurs over open land with higher SH compared to adjacent forests in the tropics, whereas cloud inhibition occurs over open land with lower SH than surrounding forests in boreal areas. Additionally, the magnitude of secondary circulations and their impact on clouds may change diurnally, driven by differential heating contrast in the diurnally varying land surface heat fluxes between adjacent patches with different land covers[55].

The type of land cover notably influences cloud formation processes by affecting surface heating, moisture availability, and atmospheric stability[56–58]. Forests generally promote cloud formation due to high moisture levels and low albedo[22], while over deserts, typically fewer clouds form, due to low moisture availability and high albedo[59]. Grasslands have a moderate effect on cloud formation that is intermediate between forests and deserts[23]. Urban areas, with their unique heat island effect and pollution, potentially influence cloud properties and formation[60]. The varying impacts of various land covers on cloud formation also explain why the results of the two methods differ. The CMIP6 models only consider deforestation into grassland, whereas the diverse land covers between adjacent ERA5 grids disrupt the signals.

Implications for radiation and climate

Previous studies have concentrated on alterations in surface albedo following deforestation, yet there is a lack of quantitative analysis on changes in cloud albedo subsequent to deforestation[22]. Clouds, on average, exert a cooling effect on climate[61]. The decrease in cloud cover with deforestation, therefore, implies a warming effect on climate. The increase in surface albedo resulting from deforestation, in turn, contributes to a cooler climate[17]. Hence, clarifying the competitive relationship between these two elements is essential to the area of forest biophysical effects.

For a complete analysis, we also examine the disturbance of the outgoing radiation at the top of the atmosphere (TOA). The perturbation of outgoing radiation under all-sky conditions reflects the combined impacts of alterations in both surface and cloud properties from deforestation. Under clear-sky conditions, the radiation perturbations solely arise from alterations in surface properties. Thus, the alterations in TOA outgoing radiation due to cloud cover changes can be obtained through the difference between all-sky and clear-sky conditions (all-sky minus clear-sky, also known as cloud radiative effect). As denoted in Fig. 3, a universal pattern prevails worldwide: alterations in surface properties largely govern the overall outgoing radiation changes, with changes in cloud cover acting as a buffer. On average, from the CMIP6 idealized deforestation experiments, reduced cloud cover offsets approximately 44% of the surface albedo cooling effect; while from the space-for-time substitution method based on ERA5, the relative offset is about 26% (Fig. 3g). The disparities in numerical outcomes primarily result from methodological differences. Nonetheless, both methods lead to consistent conclusions. Given the saturation of CMIP6 latitudinal data, we proceed to examine the zonal disparities (Fig. 3h). The discernible result reveals that the compensatory impact of cloud cover compared to the surface albedo change is stable across latitudes, at roughly 50%.

When comparing the shortwave and longwave components (Supplementary Figs. 8, 9), however, it becomes evident that the perturbations to the climate come mainly from shortwave, further indicating that changes in surface and cloud albedo are the most main causes. From a global average standpoint, the quantitative competition between clouds and surface albedo becomes apparent, showing that deforestation-induced reduction in cloudy-sky albedo partially counteracts the increased surface albedo by nearly half (Supplementary Fig. 10). Considering that alterations in cloud cover following deforestation approximately counterbalance half of the cooling effect caused by changes in surface albedo, neglecting the shifts in cloud-climate interactions introduces a large bias when investigating the biophysical effects of forests in the future.

Methods

CMIP6 simulations

Cloud fraction profile, tree cover fraction, surface LH, surface SH, surface temperature, surface radiation fluxes, surface ET, near-surface wind speed, near-surface air temperature, as well as radiation fluxes at the TOA from five GCMs (Table S1) participating in the CMIP6 are adopted in this study[35]. The idealized global deforestation simulations (deforest-glob) from the LUMIP[36] are analyzed in comparison to the pre-industrial control simulations (piControl). The deforest-glob setup assumes that a total forest area of 20 million km^2 is linearly removed from the top 30% forested area with a fixed rate of 400,000 $km^2\,yr^{-1}$ over a period of 50 years across the globe. This is then followed by at least a 30-year simulation with a constant land cover to achieve stable conditions. The last 30 years of the deforest-glob and piControl simulations are compared (deforest-glob minus piControl) to derive the mean response to deforestation[28]. Due to differences in resolution among GCMs, the ensemble mean statistics are calculated by bilinear remapping of diagnostics from individual GCMs to a $2° \times 2°$ grid, and vertically to 27 pressure levels from 1000 to 100 hPa.

Reanalysis datasets

From the ECMWF ERA5[62], we utilize the cloud fraction profiles data alongside elevation, surface LH, surface SH, surface temperature, surface radiation fluxes, surface ET, 10-m wind speed, 2-m air temperature, and TOA radiation fluxes to examine the impacts of deforestation. Datasets spanning from 2001 to 2021, featuring a spatial resolution of $0.25° \times 0.25°$ and encompassing 28 vertical pressure levels from 1000 to 100 hPa, are employed for the analysis.

Observed land cover

For delineating forested and open land areas, we use land cover data from the MODIS dataset (MCD12C1, version 6.1)[63], relying on the International Geosphere-Biosphere Program (IGBP) classification layer to define the land cover types. Annual data for the years 2001–2021 with a spatial resolution of $0.05° \times 0.05°$ are adopted. Here, five forest types (evergreen needleleaf forest, evergreen broadleaf forest, deciduous needleleaf forest, deciduous broadleaf forest, and mixed forest) are merged into a single forest classification. The forest fraction is bilinearly gridded spatially into $0.25° \times 0.25°$ to align with the ERA5 data.

Observed cloud profile and cloud top pressure

In assessing the accuracy of ERA5 cloud profiles, we analyse active satellite-observed cloud profiles. The cloud profile retrievals from Cloud-Aerosol Lidar and Infrared Pathfinder Satellite Observations (CALIPSO) and CloudSat between 2007 and 2010, are aggregated to a spatial resolution of $2° \times 2°$ and a vertical resolution of 480 m[64]. The fusion of data from both sensors facilitates an extensive depiction of the vertical cloud structure. This comprehensive view is achieved by leveraging the distinct wavelengths each sensor employs (CloudSat: ~2 mm, CALIPSO: 532 and 1064 nm), catering to various cloud and precipitation particles in both liquid and solid phases.

The International Satellite Cloud Climatology Project (ISCCP)-HGM[65] monthly average data with a spatial resolution of $1° \times 1°$ from 2001 to 2016 is employed to obtain the observed cloud top pressure for iced convective clouds. The zonal average ISCCP cloud top pressure is interpolated to GCMs or ERA5 pressure levels.

Climate zones

In this study, climate zones are defined according to the global maps of the Köppen–Geiger climate classification (Version 1)[66]. The Köppen–Geiger historical map contains 30 climate zones at a resolution of 1 km. Tropical and boreal regions are each merged from corresponding subdivided climate zones.

Extracting local effect from GCMs

Deforestation exerts a local impact on the climate within deforested areas (local effect) by modifying land surface characteristics such as albedo, roughness, and ET. Additionally, it affects both deforested and open land grids by altering the advection of heat and moisture, as well as influencing atmospheric circulation (non-local effect)[67]. Distinguishing between local and non-local effects within GCMs is crucial as coupled models encompass the complete climate response to deforestation, incorporating both local and non-local impacts. Moreover, it allows to develop a more profound insight into the mechanisms influencing the local effects in comparison to those governing the non-local effects. Mesoscale processes typically have spatial scales between 10 and 1000 km. In the CMIP6 models, mesoscale circulations within the analysis resolution (10–200 km) are partly local, while the larger ones (200–1000 km) are considered non-local. Therefore, we assume that the term "non-local effect" in the GCMs refers to both the large-scale circulations (>1000 km) and the mesoscale circulations beyond the analysis resolution (200–1000 km).

Here, we use a chessboard method as outlined by ref. 34 to assess the local effect. This method assumes that the unaltered and adjacent

deforested grids share the same non-local effect[21,67]. The unaltered grids indicate that the forest cover within these grids remains unchanged in the deforest-glob simulation. Since the cloud cover changes within unaltered forest cover grids are entirely due to non-local effects, to generate a global map of the non-local effect, we determine the non-local effects within the deforestation grid by interpolating the signals from the surrounding unaltered forest cover grids. As spatial interpolation might alter existing values, we maintain the non-local signals within the unchanged forest cover grids as they are and only derive the non-local signals for the deforested grids. The local effect over the deforested grids thus can be derived by subtracting the interpolated non-local effect from the total effect. Notably, employing a chessboard-like method introduces horizontal interpolation errors, given that the local effect relies solely on interpolation from neighboring, unaltered grids. However, our study is centered on idealized deforestation scenarios, and prior study[24], has demonstrated the possibility of isolating local effects using similar methodologies and datasets. Winckler, et al.[34] conducted comparisons between simulations involving both sparse and extensive idealized deforestation, finding small differences in derived local effects from spatial interpolation. The difference between the two local effects of sparse and extensive deforestation simulations is of secondary importance as compared to the local effect itself. Additionally, by comparing the local and non-local effects of SAT as an example (Supplementary Fig. 11), we find that both effects are non-negligible relative to the total effect. Therefore, the calculated local effect is unlikely to introduce large uncertainties due to discrepancies in magnitudes with the non-local effect.

To mitigate uncertainties, we use ensemble mean results from five available GCMs. Grid points where four or more of the five models exhibited the same sign are highlighted to demonstrate where there is a high consistency among the models. However, it should be noted that since the model results are derived from idealized deforestation experiments, they may appear overly simplistic compared to observations.

Space-for-time substitution

In addition to idealized deforestation simulations, this study employs a space-for-time substitution method to assess the impacts of deforestation, combining MODIS land cover and ERA5 reanalysis datasets. Such an approach has previously been applied in various studies to evaluate the effect of alterations in land cover on temperature[8,26], the surface energy budget[5,68], or cloud cover[21,22]. The fundamental premise of this method is that neighboring land patches share the same climatic background, and variations in their characteristics can act as a proxy for temporal changes. This method exclusively includes the local effects, comprising two components: one is the mean-state difference—variations in land cover conditions that result in spatial disparities; another is the secondary mesoscale circulation within the moving window pixels —differential heating of adjacent land cover patches can create sea-breeze-like secondary mesoscale circulations[21,23,55]. However, it should be acknowledged that the space-for-time substitution approach also carries uncertainties as it is an indirect method to calculate local biophysical effects.

Areas designated as unaltered forested (or unaltered open land) are identified as pixels where the initial (in 2001) tree cover fraction exceeds 60% (or is below 40%) and with a net change in forest cover <10% from 2001 to 2021. Pixels with water coverage >10% are excluded. We use a moving window approach to search for comparison samples between unaltered forested and unaltered open land pixels. We choose for each moving window a size of 7 × 7 pixels (1.75° × 1.75°). To reduce the influence of topography[69,70], we calculate the standard deviation (s.d.) of elevation within specific moving windows and omit samples where this s.d. exceeds 100 m following ref. 21. Finally, the potential effect of deforestation on a specific variable (ΔVar) is quantified as:

$$\Delta \text{Var} = \text{Var}_{\text{open land}} - \overline{\text{Var}_{\text{surrounding forests}}} \tag{1}$$

or

$$\Delta \text{Var} = \overline{\text{Var}_{\text{surrounding open lands}}} - \text{Var}_{\text{forest}} \tag{2}$$

where Eqs. (1) and (2) are applicable to the case where the central pixel of the moving window is unaltered open land and unaltered forest, respectively. $\text{Var}_{\text{open land}}$ and $\text{Var}_{\text{forest}}$ are multi-year mean variables over unaltered open land and unaltered forest pixels, respectively. $\overline{\text{Var}_{\text{surrounding forests}}}$ and $\overline{\text{Var}_{\text{surrounding open lands}}}$ are the average values of the surrounding $\text{Var}_{\text{forest}}$ and $\text{Var}_{\text{open land}}$ within a moving window when the central pixel is unaltered open land and unaltered forest, respectively.

Data availability

Code availability

References

1. Bonan, G. B. Forests and climate change: forcings, feedbacks, and the climate benefits of forests. *Science* **320**, 1444–1449 (2008).
2. Nabuurs, G.-J. et al. First signs of carbon sink saturation in European forest biomass. *Nat. Clim. Change* **3**, 792–796 (2013).
3. Baccini, A. et al. Estimated carbon dioxide emissions from tropical deforestation improved by carbon-density maps. *Nat. Clim. Change* **2**, 182–185 (2012).
4. Runyan, C. W., D'Odorico, P. & Lawrence, D. Physical and biological feedbacks of deforestation. *Rev. Geophys.* https://doi.org/10.1029/2012RG000394 (2012).
5. Duveiller, G., Hooker, J. & Cescatti, A. The mark of vegetation change on Earth's surface energy balance. *Nat. Commun.* **9**, 679 (2018).
6. Perugini, L. et al. Biophysical effects on temperature and precipitation due to land cover change. *Environ. Res. Lett.* **12**, 053002 (2017).
7. Bright, R. M. et al. Local temperature response to land cover and management change driven by non-radiative processes. *Nat. Clim. Change* **7**, 296–302 (2017).
8. Li, Y. et al. Local cooling and warming effects of forests based on satellite observations. *Nat. Commun.* **6**, 6603 (2015).
9. Lee, X. et al. Observed increase in local cooling effect of deforestation at higher latitudes. *Nature* **479**, 384–387 (2011).

10. Williams, C. A., Gu, H. & Jiao, T. Climate impacts of U.S. forest loss span net warming to net cooling. *Sci. Adv.* **7**, eaax8859 (2021).

11. Bala, G. et al. Combined climate and carbon-cycle effects of large-scale deforestation. *Proc. Natl Acad. Sci. USA* **104**, 6550–6555 (2007).

12. Betts, R. A. Offset of the potential carbon sink from boreal forestation by decreases in surface albedo. *Nature* **408**, 187–190 (2000).

13. Claussen, M., Brovkin, V. & Ganopolski, A. Biogeophysical versus biogeochemical feedbacks of large-scale land cover change. *Geophys. Res. Lett.* **28**, 1011–1014 (2001).

14. Arora, V. K. & Montenegro, A. Small temperature benefits provided by realistic afforestation efforts. *Nat. Geosci.* **4**, 514–518 (2011).

15. Li, Y. et al. Deforestation-induced climate change reduces carbon storage in remaining tropical forests. *Nat. Commun.* **13**, 1964 (2022).

16. Windisch, M. G., Davin, E. L. & Seneviratne, S. I. Prioritizing forestation based on biogeochemical and local biogeophysical impacts. *Nat. Clim. Change* **11**, 867–871 (2021).

17. Davin, E. L. & de Noblet-Ducoudré, N. Climatic impact of global-scale deforestation: radiative versus nonradiative processes. *J. Clim.* **23**, 97–112 (2010).

18. Snyder, P. K., Delire, C. & Foley, J. A. Evaluating the influence of different vegetation biomes on the global climate. *Clim. Dyn.* **23**, 279–302 (2004).

19. Zhang, M. et al. Response of surface air temperature to small-scale land clearing across latitudes. *Environ. Res. Lett.* **9**, 034002 (2014).

20. Norris, J. R. et al. Evidence for climate change in the satellite cloud record. *Nature* **536**, 72–75 (2016).

21. Xu, R. et al. Contrasting impacts of forests on cloud cover based on satellite observations. *Nat. Commun.* **13**, 670 (2022).

22. Duveiller, G. et al. Revealing the widespread potential of forests to increase low level cloud cover. *Nat. Commun.* **12**, 4337 (2021).

23. Teuling, A. J. et al. Observational evidence for cloud cover enhancement over western European forests. *Nat. Commun.* **8**, 14065 (2017).

24. Hua, W., Zhou, L., Dai, A., Chen, H. & Liu, Y. Important non-local effects of deforestation on cloud cover changes in CMIP6 models. *Environ. Res. Lett.* **18**, 094047 (2023).

25. Cerasoli, S., Yin, J. & Porporato, A. Cloud cooling effects of afforestation and reforestation at midlatitudes. *Proc. Natl Acad. Sci. USA* **118**, e2026241118 (2021).

26. Chen, L. & Dirmeyer, P. A. Reconciling the disagreement between observed and simulated temperature responses to deforestation. *Nat. Commun.* **11**, 202 (2020).

27. Ge, J. et al. Local surface cooling from afforestation amplified by lower aerosol pollution. *Nat. Geosci.* **16**, 781–788 (2023).

28. Boysen, L. R. et al. Global climate response to idealized deforestation in CMIP6 models. *Biogeosciences* **17**, 5615–5638 (2020).

29. Portmann, R. et al. Global forestation and deforestation affect remote climate via adjusted atmosphere and ocean circulation. *Nat. Commun.* **13**, 5569 (2022).

30. Luo, H., Quaas, J. & Han, Y. Examining cloud vertical structure and radiative effects from satellite retrievals and evaluation of CMIP6 scenarios. *Atmos. Chem. Phys.* **23**, 8169–8186 (2023).

31. Chen, T., Rossow, W. B. & Zhang, Y. Radiative effects of cloud-type variations. *J. Clim.* **13**, 264–286 (2000).

32. Slingo, A. Sensitivity of the Earth's radiation budget to changes in low clouds. *Nature* **343**, 49–51 (1990).

33. Lohmann, U. & Roeckner, E. Influence of cirrus cloud radiative forcing on climate and climate sensitivity in a general circulation model. *J. Geophys. Res.* **100**, 16305–16323 (1995).

34. Winckler, J., Reick, C. H. & Pongratz, J. Robust identification of local biogeophysical effects of land-cover change in a global climate model. *J. Clim.* **30**, 1159–1176 (2017).

35. Eyring, V. et al. Overview of the coupled model intercomparison project phase 6 (CMIP6) experimental design and organization. *Geosci. Model Dev.* **9**, 1937–1958 (2016).

36. Lawrence, D. M. et al. The Land Use Model Intercomparison Project (LUMIP) contribution to CMIP6: rationale and experimental design. *Geosci. Model Dev.* **9**, 2973–2998 (2016).

37. Blanchard, Y. et al. A synergistic analysis of cloud cover and vertical distribution from A-train and ground-based sensors over the high Arctic station Eureka from 2006 to 2010. *J. Appl. Meteorol. Climatol.* **53**, 2553–2570 (2014).

38. Christensen, M. W., Stephens, G. L. & Lebsock, M. D. Exposing biases in retrieved low cloud properties from CloudSat: a guide for evaluating observations and climate data. *J. Geophys. Res.* **118**, 12,120–12,131 (2013).

39. Liu, Y. Impacts of active satellite sensors' low-level cloud detection limitations on cloud radiative forcing in the Arctic. *Atmos. Chem. Phys.* **22**, 8151–8173 (2022).

40. Winker, D. M. et al. Overview of the CALIPSO mission and CALIOP data processing algorithms. *J. Atmos. Ocean. Technol.* **26**, 2310–2323 (2009).

41. Betts, A. K. Land-surface-atmosphere coupling in observations and models. *J. Adv. Model. Earth Syst.* **1**, 4 (2009).

42. Teixeira, J. & Hogan, T. F. Boundary layer clouds in a global atmospheric model: simple cloud cover parameterizations. *J. Clim.* **15**, 1261–1276 (2002).

43. Su, T., Li, Z., Zhang, Y., Zheng, Y. & Zhang, H. Observation and reanalysis derived relationships between cloud and land surface fluxes across cumulus and stratiform coupling over the southern Great Plains. *Geophys. Res. Lett.* **51**, e2023GL108090 (2024).

44. Wu, C.-M., Stevens, B. & Arakawa, A. What controls the transition from shallow to deep convection? *J. Atmos. Sci.* **66**, 1793–1806 (2009).

45. Schumacher, R. S. & Rasmussen, K. L. The formation, character and changing nature of mesoscale convective systems. *Nat. Rev. Earth Environ.* **1**, 300–314 (2020).

46. Bony, S. et al. Clouds, circulation and climate sensitivity. *Nat. Geosci.* **8**, 261–268 (2015).

47. Wang, J. et al. Impact of deforestation in the Amazon basin on cloud climatology. *Proc. Natl Acad. Sci. USA* **106**, 3670–3674 (2009).

48. Sherwood, S. C., Roca, R., Weckwerth, T. M. & Andronova, N. G. Tropospheric water vapor, convection, and climate. *Rev. Geophys.* **48**, RG2001 (2010).

49. Lawrence, D., Coe, M., Walker, W., Verchot, L. & Vandecar, K. The unseen effects of deforestation: biophysical effects on climate. *Front. For. Glob. Change* **5**, 756115 (2022).

50. De Hertog, S. J. et al. The biogeophysical effects of idealized land cover and land management changes in Earth system models. *Earth Syst. Dyn.* **14**, 629–667 (2023).

51. Su, Y. et al. Asymmetric influence of forest cover gain and loss on land surface temperature. *Nat. Clim. Change* **13**, 823–831 (2023).

52. Alkama, R. & Cescatti, A. Biophysical climate impacts of recent changes in global forest cover. *Science* **351**, 600–604 (2016).

53. Fairall, C. W., Bradley, E. F., Hare, J. E., Grachev, A. A. & Edson, J. B. Bulk parameterization of air–sea fluxes: updates and verification for the COARE algorithm. *J. Clim.* **16**, 571–591 (2003).

54. Liao, W. et al. Sensitivities and responses of land surface temperature to deforestation-induced biophysical changes in two global Earth system models. *J. Clim.* **33**, 8381–8399 (2020).

55. Tian, J., Zhang, Y., Klein, S. A., Öktem, R. & Wang, L. How does land cover and its heterogeneity length scales affect the formation of summertime shallow cumulus clouds in observations from the US southern Great Plains? *Geophys. Res. Lett.* **49**, e2021GL097070 (2022).

56. Mahmood, R. et al. Land cover changes and their biogeophysical effects on climate. *Int. J. Climatol.* **34**, 929–953 (2014).
57. Pielke, R. A. Sr. et al. Land use/land cover changes and climate: modeling analysis and observational evidence. *WIREs Clim. Change* **2**, 828–850 (2011).
58. Rabin, R. M., Stadler, S., Wetzel, P. J., Stensrud, D. J. & Gregory, M. Observed effects of landscape variability on convective clouds. *Bull. Am. Meteorol. Soc.* **71**, 272–280 (1990).
59. Rosenfeld, D., Rudich, Y. & Lahav, R. Desert dust suppressing precipitation: a possible desertification feedback loop. *Proc. Natl Acad. Sci. USA* **98**, 5975–5980 (2001).
60. Vo, T. T., Hu, L., Xue, L., Li, Q. & Chen, S. Urban effects on local cloud patterns. *Proc. Natl Acad. Sci. USA* **120**, e2216765120 (2023).
61. Zelinka, M. D., Randall, D. A., Webb, M. J. & Klein, S. A. Clearing clouds of uncertainty. *Nat. Clim. Change* **7**, 674–678 (2017).
62. Hersbach, H. et al. The ERA5 global reanalysis. *Q. J. R. Meteorol. Soc.* **146**, 1999–2049 (2020).
63. Sulla-Menashe, D., Gray, J. M., Abercrombie, S. P. & Friedl, M. A. Hierarchical mapping of annual global land cover 2001 to present: the MODIS collection 6 land cover product. *Remote Sens. Environ.* **222**, 183–194 (2019).
64. Kay, J. E. & Gettelman, A. Cloud influence on and response to seasonal Arctic sea ice loss. *J. Geophys. Res.* **114**, D18204 (2009).
65. Young, A. H., Knapp, K. R., Inamdar, A., Hankins, W. & Rossow, W. B. The International Satellite Cloud Climatology Project H-Series climate data record product. *Earth Syst. Sci. Data* **10**, 583–593 (2018).
66. Beck, H. E. et al. Present and future Köppen-Geiger climate classification maps at 1-km resolution. *Sci. Data* **5**, 180214 (2018).
67. Pongratz, J. et al. Land use effects on climate: current state, recent progress, and emerging topics. *Curr. Clim. Change Rep.* **7**, 99–120 (2021).
68. Liu, Z., Ballantyne, A. P. & Cooper, L. A. Biophysical feedback of global forest fires on surface temperature. *Nat. Commun.* **10**, 214 (2019).
69. Nair, U. S., Lawton, R. O., Welch, R. M. & Pielke, R. A. Sr. Impact of land use on Costa Rican tropical montane cloud forests: Sensitivity of cumulus cloud field characteristics to lowland deforestation. *J. Geophys. Res.* **108**, 4206 (2003).
70. Ray, D. K., Nair, U. S., Lawton, R. O., Welch, R. M. & Pielke, R. A. Sr. Impact of land use on Costa Rican tropical montane cloud forests: Sensitivity of orographic cloud formation to deforestation in the plains. *J. Geophys. Res.* **111**, D02108 (2006).

Acknowledgements

Author contributions

J.Q., H.L., and Y.H. designed the research. H.L. performed the research and drafted the paper. H.L., J.Q., and Y.H. contributed to analysis and interpretation of the results, as well as revising the paper.

Competing interests

The authors declare no competing interests.

Additional information

Supplementary information The online version contains supplementary material available at https://doi.org/10.1038/s41467-024-51783-y.

Correspondence and requests for materials should be addressed to Hao Luo or Yong Han.

Peer review information *Nature Communications* thanks Adriaan J. Teuling and the other, anonymous, reviewer for their contribution to the peer review of this work. A peer review file is available.

Reprints and permissions information is available at http://www.nature.com/reprints

Publisher's note Springer Nature remains neutral with regard to jurisdictional claims in published maps and institutional affiliations.